Spectroscopic properties of ytterbium, praseodymium-codoped fluorozirconate glass for laser emission at 3.6 μm

Laércio Gomes[1] and Stuart D. Jackson[2,*]

[1]*Center for Lasers and Applications, IPEN/CNEN-SP, P.O. Box 11049, São Paulo 05422-970, Brazil*
[2]*Institute of Photonics and Optical Science, School of Physics, University of Sydney, Camperdown, New South Wales 2006, Australia*
**Corresponding author: stuart.jackson@sydney.edu.au*

Received December 13, 2012; revised March 7, 2013; accepted March 29, 2013; posted March 29, 2013 (Doc. ID 181707); published May 2, 2013

Excitation of the $^2F_{7/2} \rightarrow {}^2F_{5/2}$ transition of the Yb^{3+} ion in Yb^{3+}, Pr^{3+}-doped fluorozirconate glass at 974 nm results in efficient excitation of the $^1G_4$ level of Pr^{3+} ion that in turn emits in the middle infrared at ~3.6 μm. The energy transfer (ET) process $Yb^{3+}(^2F_{5/2}) \rightarrow Pr^{3+}(^1G_4)$ is assisted by fast excitation migration among the Yb^{3+} ions. An upconversion process involving ET from the $^2F_{5/2}$ level to the $^1G_4$ excited state populates the $^3P_0$ excited state that produces emission at 481, 521, 603, 636, and 717 nm. A study of the behavior of the fluorescence from the $^1G_4$ level at 1325 nm and from the $^3P_0$ level at 603 nm allowed the estimation of the ET rate constants for the processes involved after short-pulsed laser excitation at 974 nm. A rate-equation model was employed to evaluate the population inversion relating to the $^1G_4 \rightarrow {}^3F_4$ transition of the Pr^{3+} ion at 3.6 μm under continuous wave pumping.

OCIS codes: (300.0300) Spectroscopy; (140.3510) Lasers, fiber.
http://dx.doi.org/10.1364/JOSAB.30.001410

1. INTRODUCTION

Generating light from in the middle infrared region of the electromagnetic spectrum from a fiber laser source is currently an area of immense interest. To date, the fluoride glasses are the most researched because these glasses have good transmission properties, they can be doped to moderately high rare earth concentration, and importantly they are commercially available from a number of sources. To date, most of the research has focused on the 3 μm transitions of Er^{3+} [1] and Ho^{3+} [2], which can be diode pumped and produce output at near Stokes-limited efficiencies. The demonstration of longer wavelength emission up to 3.9 μm from a Ho^{3+}-doped fluoride glass fiber laser [3] shows that there are opportunities for moderate output power emission from fiber lasers up to this wavelength limit using transitions that are conveniently accessed using diode laser pumping.

The $^1G_4 \rightarrow {}^3F_4$ transition of Pr^{3+} is a four-level laser transition that offers broadband fluorescence in the 3.6 μm region of the mid-infrared spectrum. Unfortunately, Pr^{3+} is not easily pumped with commercially available diode lasers and therefore requires a sensitizer ion, which can transfer energy and enable excitation of the $^1G_4$ energy level. A suitable sensitizer is the Yb^{3+} ion, which is a well-understood rare earth ion dopant for fluoride glass that displays strong absorption and emission cross sections in the 1 μm region of the near infrared spectrum that is suitable for diode pumping at 976 nm and subsequent energy transfer (ET) to the $^1G_4$ level of the Pr^{3+} ion. The strong absorption of Yb^{3+} ions at 974 nm that efficiently excites the $^1G_4$ level of Pr^{3+} ions by way of ET has been investigated previously in fluorides crystals [4–7]. This has allowed generation of stimulated emission in two new channels from Stark levels of the $^1G_4$ manifold, one of which is the $^1G_4 \rightarrow {}^3F_4$ transition that emits at about 3.6 μm [6].

To explore the potential of this transition to supply gain for fiber lasers for emission at 3.6 μm, detailed spectroscopic studies are required that will reveal the important ET and energy level decay processes that relate to the $^1G_4 \rightarrow {}^3F_4$ transition of the Pr^{3+} ion in Yb^{3+}, Pr^{3+}-doped fluorozirconate (ZBLAN) glass. To fulfill this objective, we have prepared a number of $Yb^{3+}(x)$, Pr^{3+}(1 mol. %)-doped ZBLAN glasses of varying Yb^{3+} concentrations ($x = 1$, 2, 3, 4, and 5 mol. %) and measured the luminescence decay characteristics after selective energy level excitation. The luminescence efficiencies of these levels were determined when the experimental decay time was compared with the calculated radiative lifetimes. Measurements of pump upconversion luminescence from the $^1G_4$ level to the $^3P_0$ level after excitation at 974 nm was carried out. The results from a numerical simulation that solved the relevant rate equations showed that a population inversion is reached for the laser transition at 3.6 μm in Yb^{3+}, Pr^{3+}-doped ZBLAN glass at a relatively modest threshold pumping intensity for CW laser pumping at 970 nm.

2. EXPERIMENTAL PROCEDURE

The ZBLAN glass samples used for the time-resolved luminescence spectroscopy measurements were prepared from ultrapure fluoride starting materials and made with the composition: $(99 - x - y)$ [$53ZrF_4$–$20BaF_2$–$4LaF_3$–$20NaF$] – $x[YbF_3]$–$y[PrF_3]$ with $x = 1$, 2, 3, 4, 5 mol. % and $y = 1$ mol. %. The starting powder materials were melted at 850°C for 120 min

in a Pt–Au crucible. The liquids were poured into brass molds and annealed at 260°C for 2 h to remove the mechanical stresses. The samples were cut and polished into $15 \times 12 \times 8$ mm rectangular prisms.

Absorption spectra in the range of 400–1100 nm were measured using a Cary 5000 spectrophotometer. The decay characteristics of the excited states of the Yb^{3+} and Pr^{3+} ions were measured using pulsed 12 mJ and 4 ns laser excitation from a tunable optical parametric oscillator (OPO) pumped by the second harmonic of a *Q*-switched Nd-YAG laser (Brilliant *B* from Quantel). Tunable laser excitation from the OPO was used to directly excite the $^2F_{5/2}$ energy level of Yb^{3+} at 970 nm and the $^3P_0$ energy level of Pr^{3+} at 480 nm. The infrared luminescence was detected using an InSb infrared detector (Judson model J-10D cooled to 77 K) in conjunction with a fast preamplifier with a response time of ~0.5 μs and analyzed using a digital 200 MHz oscilloscope (Tektronix TDS 410). Visible luminescence was detected using a photomultiplier tube with a S-20 type cathode cooled to −20°C. All the fluorescence decay characteristics were measured at 300 K. To isolate the luminescence signals, bandpass filters each with ~80% transmission at 1310 nm with a half-width of 25 nm and an extinction coefficient of $\sim 10^{-5}$ outside this band were used. For the luminescence spectrum measurements from the visible to the mid-infrared, a 0.25 m monochromator with optical gratings blazed for 500, 1000, or 2600 nm were used.

3. EXPERIMENTAL RESULTS

The optical absorption spectrum of the Yb^{3+} and Pr^{3+} ions when doped into ZBLAN glass has one main absorption peak in the near infrared at around 975 nm (from Yb^{3+}) and 1020 nm (from Pr^{3+}), as shown in Fig. 1. The absorption spectrum of Yb^{3+}(3 mol. %), Pr^{3+}(1 mol. %)-doped ZBLAN is shown in Fig. 1 as the black line, where one can see that the absorption peak of Yb^{3+} occurs at 975 nm with an absorption coefficient $\alpha = 4.23$ cm^{-1}. Using the Yb^{3+} ion concentration $N = 4.125 \times 10^{20}$ ions cm^{-3} (3 mol. %) in the relation $\alpha = N\sigma_{Abs}$, we get the maximum absorption cross section calculated to be 1.025×10^{-20} cm^2. One can observe that the absorption peak for the $^3H_4 \rightarrow {}^1G_4$ transition of Pr^{3+} occurs at 1017 nm with $\alpha = 0.083$ cm^{-1} providing a peak absorption cross section of 6.04×10^{-22} cm^2.

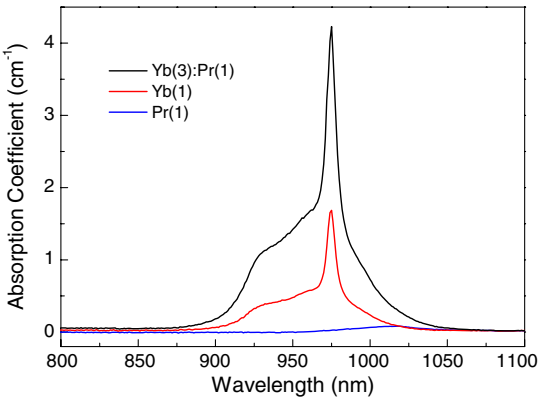

Fig. 1. Measured absorption spectrum of Yb^{3+}(1 mol. %), Pr^{3+}(1 mol. %) and Yb^{3+}(3 mol. %), Pr^{3+}(1 mol. %)-doped ZBLAN. The absorption cross section of Yb^{3+} is equal to 1.025×10^{-20} cm^2 at 975 nm and the absorption cross section of Pr^{3+} is equal to 6.04×10^{-22} cm^2 at 1017 nm.

The infrared and mid-infrared emission spectra measured for Yb^{3+}(5 mol. %), Pr^{3+}(1 mol. %))-doped ZBLAN is shown in Fig. 2. Short pulse laser excitation at 974 nm ($E \sim 14$ mJ, 4 ns) was used to induce the luminescence and a box-car integrator technique was employed to process the luminescence signals. An optical grating blazed at 2.6 μm was used in the monochromator. A silicon (Si) filter was used in front of the monochromator entrance for measuring the 1.35 μm emission and a germanium (Ge) filter was used for measuring the mid-infrared emissions.

The midwave infrared emission from the $^1G_4$ level of Pr^{3+} comprises a wide band ranging from 3.1 to 3.9 μm with a mean emission wavelength at approximately 3.57 μm. The emission shows two peaks, one located at ~3.44 μm due to the $^1G_4 \rightarrow {}^3F_3$ transition and the other located at ~3.69 μm resulting from the $^1G_4 \rightarrow {}^3F_4$ transition. The ~3.6 μm emission was easily detected at 300 K in the $Yb^{3+}(x)$, Pr^{3+}(1 mol. %)-doped ZBLAN samples with laser excitation at 974 nm but was not detectable in singly Pr^{3+}(1 mol. %)-doped ZBLAN with laser excitation from 970 to 1020 nm due to the small absorption cross section of the $^3H_4 \rightarrow {}^1G_4$ transition. Laser excitation at 442 nm was employed to indirectly excite the $^1G_4$ level by way of the $^3H_4 \rightarrow {}^3P_0$ absorption transition in order to measure the intrinsic decay the $^1G_4$ level in singly doped Pr^{3+}(1 mol. %)) samples and the effects on the $^1G_4$ level decay on the presence of Yb^{3+} in the Yb(x): Pr(1 mol. %)-codoped samples.

When the Yb^{3+}, Pr^{3+}-doped ZBLAN glass is excited at 974 nm, the following processes are thought to occur:

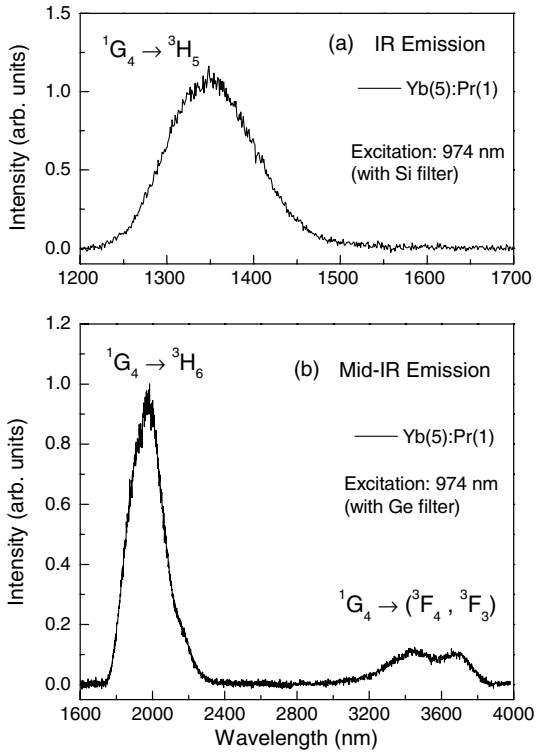

Fig. 2. Measured mid-infrared emission spectrum of Yb^{3+}(5 mol. %), Pr^{3+}(1 mol. %)-doped ZBLAN measured using a box-car integrator and an InSb detector (cooled to 77 K) with a fast pre-amplifier and a 974 nm pulsed laser excitation of 4 ns duration time and 10 Hz. The emission intensities were not corrected for grating efficiency. The emission cross section at 3690 nm (i.e., the second peak) was calculated to be 5.76×10^{-21} cm^2.

(a) Ground state absorption (GSA)

$$Yb^{3+}(^2F_{7/2}) + h\nu(974\ \text{nm}) \rightarrow Yb^{3+}(^2F_{5/2}),$$

(b) Energy transfer (ET)

$$Yb^{3+}(^2F_{5/2}) + Pr^{3+}(^3H_4) \rightarrow Yb^{3+}(^2F_{7/2}) + Pr^{3+}(^1G_4),$$

(c) Back-transfer (BT)

$$Pr^{3+}(^1G_4) + Yb^{3+}(^2F_{7/2}) \rightarrow Pr^{3+}(^3H_4) + Yb^{3+}(^2F_{5/2}),$$

(d) Upconversion (UP)

$$Pr^{3+}(^1G_4) + Yb^{3+} + (^2F_{5/2}) \rightarrow Pr^{3+}(^3P_0) + Yb^{3+}(^2F_{7/2}),$$

(e) Cross-relaxation (CR)

$$Pr^{3+}(^3P_0) + Yb^{3+}(^2F_{7/2}) \rightarrow Pr^{3+}(^1G_4) + Yb^{3+}(^2F_{5/2}).$$

A. Luminescence Decay of the $^2F_{5/2}$ Level

The luminescence decay characteristics of the $^2F_{5/2} \rightarrow {}^2F_{7/2}$ transition measured at 994 nm in Yb^{3+}(1 mol.%)- and Yb^{3+}(5 mol.%), Pr^{3+}(1 mol.%)-codoped ZBLAN glasses after pulsed laser excitation at 970 nm are shown in Fig. 3. Figure 3(a) shows the decay of the $^2F_{5/2}$ excited level in the Yb^{3+}(1 mol.%)-doped ZBLAN case that exhibits an exponential decay time $\tau = 2.13$ ms (τ in this case should be equal to τ_R the radiative lifetime because the multiphonon relaxation rate should be negligible). Figure 3(b) shows the decay characteristic of the $^2F_{5/2}$ level with a constant decay time $\tau =$ 52 μs obtained by integration of the normalized best-fit curve (red line) for Yb^{3+}(5 mol.%), Pr^{3+}(1 mol.%)-codoped ZBLAN system. The following decay times (τ) were obtained: 276 μs ($x = 1$ mol.%), 150 μs ($x = 2$ mol.%), 103 μs ($x = 3$ mol.%), and 72 μs for $x = 4$ mol.%. The reduction in the decay time of the $^2F_{5/2}$ level in the presence of 1 mol.% Pr^{3+} with increasing [Yb^{3+}] indicates that strong $Yb^{3+}(^2F_{5/2}) \rightarrow Pr^{3+}(^1G_4)$ ET takes place that should also be assisted by excitation migration of the $^2F_{5/2}$ states.

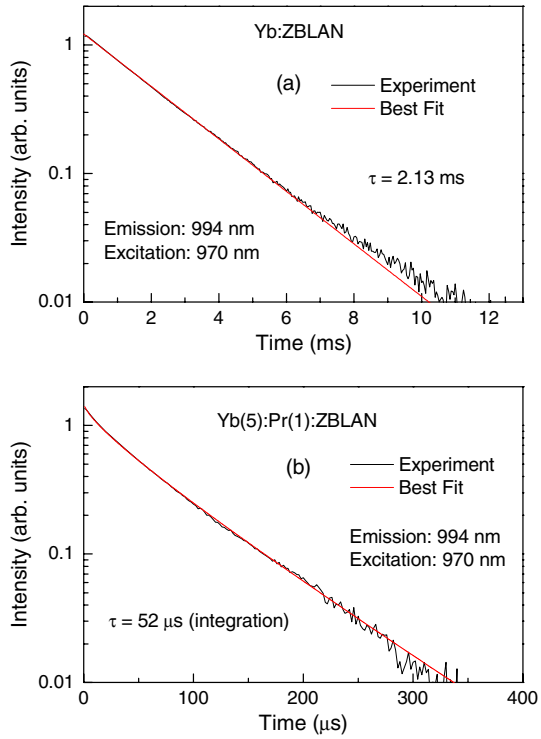

Fig. 3. Emission decay from Yb^{3+} measured at 994 nm for (a) Yb^{3+}(1 mol.%) and (b) Yb^{3+}(5 mol.%), Pr^{3+}(1 mol.%)-doped ZBLAN samples after the pulsed laser excitation at 970 nm with 4 ns and 10 Hz ($E \sim 10$ mJ).

B. Luminescence Decay of the $^1G_4$ Level

Luminescence decay characteristics of the $^1G_4$ excited level in $Yb^{3+}(x)$, Pr^{3+}(1 mol.%))-codoped ZBLAN were measured at 1310 nm after laser excitations at 442 nm (that excites Pr^{3+} ions) and 970 nm (that excites Yb^{3+} ions) at 300 K. The luminescence measurements were performed using an InSb (77 K) detector plus a narrow band pass filter with a peak transmission of 80% at 1310 nm. Figure 4 shows the 1310 nm emission measured after the Pr^{3+} ions are excited at 442 nm for the $Yb^{3+}(x)$:Pr^{3+}(1) system with $x = 0$, 1, 2, 3, 4 and 5 mol. % (colored lines), where one can see that the total decay of the $^1G_4$ level decreases with the increase in [Yb^{3+}]. To provide a better fit to the decay, we applied a time delay of $t \leq 40$ μs to the box-car integrator after the laser pulse excitation to measure the decay curve of the 1310 nm emission without interference of the luminescence risetime shown by dashed lines in Fig. 4. The emission decay curves were fitted using the Burhstein model [8] given by Eq. (1), where the best fit parameters t_1 and γ where obtained. t_1 accounts for the intrinsic decay added to the excitation migration assisted (Pr → Yb) ET and γ accounts for the direct ($Pr^{3+} \rightarrow Yb^{3+}$) transfer. Equation (1) is given by

$$I_1(t) = A\ \exp\left(-\frac{t}{t_1} - \gamma\sqrt{t}\right). \tag{1}$$

The decay time of the $^1G_4$ level was obtained by integration according to Eq. (2), which is given by

$$\tau_1 = \frac{1}{A}\int I(t)\mathrm{d}t. \tag{2}$$

The following parameters were obtained from a best fit: (i) $x = 0$ mol.%: $t_1 = 67$ μs and $\gamma = 0\ \text{s}^{-1}$ ($R^2 = 0.997$) and

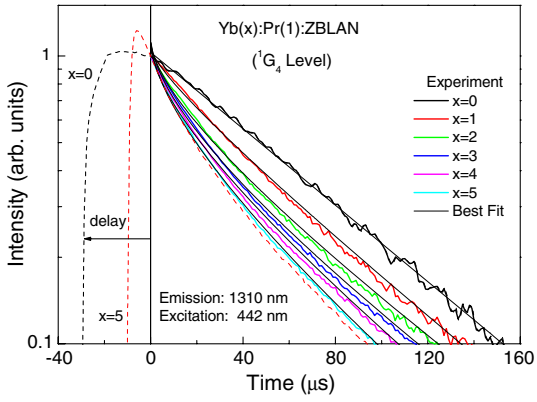

Fig. 4. Measured luminescence decay of the $^1G_4$ excited level in $Yb^{3+}(x)$, Pr^{3+}(1 mol.%)-doped ZBLAN measured at 1310 nm after the laser excitation at 442 nm at 300 K. A best fit was performed using Eq. (1). The dashed line curves show the total luminescence transient (rise and decay) for singly ($x = 0$) and codoped ($x = 5$ mol.%) samples.

Table 1. Experimental Values of the Spectroscopic Parameters of Yb^{3+}, Pr^{3+}-doped ZBLAN

Radiative Transition (level No.) (λ)	Radiative Lifetime (τ_R)[a]	Intrinsic Decay Time (τ_i) (expt.)[b]	Branching Ratio (β_{JJ}) (expt.)[b]	Multiphonon Decay W_{nR} (s^{-1})
$^3P_0 \rightarrow {}^3H_4$ (5) (481 nm)		$\tau_5 = 35$ μs	0.161	—
$^3P_0 \rightarrow {}^3H_5$ (521 nm)			0.075	
$^3P_0 \rightarrow {}^3H_6$ (603 nm)			0.295	
$^3P_0 \rightarrow {}^3F_2$ (636 nm)			0.320	
$^3P_0 \rightarrow {}^3F_4, {}^3F_3$ (718 nm)			0.075	
$^3P_0 \rightarrow {}^1G_4$ (920 nm)			$\beta_{54} = 0.074$	
$^1G_4 \rightarrow {}^3H_4$ (4) (1020 nm)	$\tau_{R4} = 2.43$ ms	$\tau_4 = 67$ μs	0.058	14514
$^1G_4 \rightarrow {}^3H_5$ (1350 nm)			0.634	
$^1G_4 \rightarrow {}^3H_6$ (1980 nm)			0.253	
$^1G_4 \rightarrow {}^3F_2$ (2120 nm)			0.0067	
$^1G_4 \rightarrow {}^3F_4, {}^3F_3$, (3570 nm)			0.0483	

Yb(x): Pr(1) (x mol. %)	Direct transfer W_T (s^{-1})[b]		Back transfer W_{BT} (s^{-1})[b]	Upconversion K_0 (s^{-1})[b]	Cross-relaxation W_{CR}(s^{-1})[b]
	Fast (45%)	Slow (55%)			
1	3.93×10^5	1.22×10^4	2526	1668	1.16×10^4
2	3.78×10^5	1.32×10^4	4798	3468	3.24×10^4
3	3.50×10^5	1.65×10^4	6861	5358	6.49×10^4
4	3.20×10^5	1.87×10^4	8439	7282	9.19×10^4
5	2.97×10^5	2.64×10^4	10650	9250	1.19×10^5

[a]Radiative lifetimes and branching ratios obtained from [11].
[b]Experimental values obtained in this work.

$\tau_1 = 67$ μs; (ii) $x = 1$ mol. %: $t_1 = 75$ μs and $\gamma = 51$ s^{-1} ($R^2 = 0.998$) and $\tau_1 = 57$ μs; (iii) $x = 2$ mol. %: $t_1 = 100$ μs and $\gamma = 108$ s^{-1} ($R^2 = 0.998$) and $\tau_1 = 51$ μs; (iv) $x = 3$ mol. %: $t_1 = 101$ μs and $\gamma = 131$ s^{-1} ($R^2 = 0.998$) and $\tau_1 = 46$ μs; (v) $x = 4$ mol. %: $t_1 = 95$ μs and $\gamma = 124$ ($R^2 = 0.997$) and $\tau_1 = 43$ μs; (vi) $x = 5$ mol. %: $t_1 = 97$ μs and $\gamma = 146$ ($R^2 = 0.999$) and $\tau_1 = 39$ μs. The rate of back ET (i.e., $Pr^{3+} \rightarrow Yb^{3+}$) was obtained using

$$W_{BT} = \frac{1}{\tau_1} - \frac{1}{\tau_i(^1G_4)}, \tag{3}$$

where τ_i ($^1G_4$) is equal to 67 μs (i.e., the intrinsic lifetime) and τ_1 is the integrated lifetime of the $^1G_4$ level. The experimental rates values of the BT (W_{BT}) are given in Table 1.

Figure 5 shows the 1310 nm emission transient measured after the Yb^{3+} ions are excited at 970 nm for the $Yb^{3+}(x)$:$Pr^{3+}(1)$ system with $x = 1$, 2, 3, 4, and 5 mol. % (colored lines), where one can see a very a fast luminescence

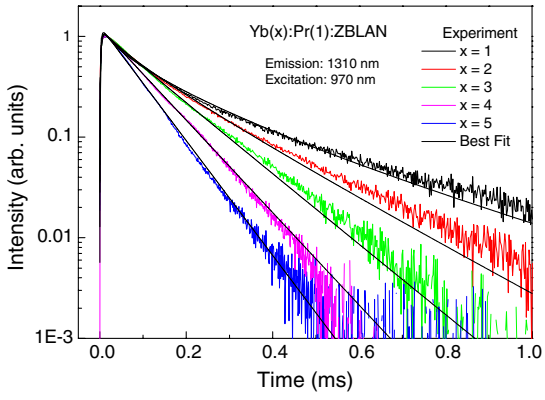

Fig. 5. Measured luminescence decay of the $^1G_4$ excited level in $Yb^{3+}(x)$, $Pr^{3+}(1$ mol. %)-doped ZBLAN measured at 1310 nm after the laser excitation at 970 nm at 300 K. A best fit was performed using Eq. (4).

risetime of ~3 μs that is related to the fast component of the $Yb^{3+} \rightarrow Pr^{3+}$ ET (i.e., fast migration). One must note that the total decay time of the $^1G_4$ level is in all the cases longer than the intrinsic lifetime of 67 μs (measured for $x = 0$ mol. %), as shown in Fig. 4, which must indicate that this effect is related to the slow component of the $Yb^{3+} \rightarrow Pr^{3+}$ ET process that contributes to the increasing decay time of the luminescence transient compared to the decay time of singly doped Pr^{3+}(1 mol. %). This contribution is dependent on [Yb^{3+}]. Curves of best fit were obtained using the time evolution of the acceptor luminescence, as given in [9], which is given by

$$I_2(t) = B\left(\exp\left(-\frac{t}{t_2} - \gamma\sqrt{t}\right) - \exp\left(-\frac{t}{t_3}\right)\right), \tag{4}$$

where the first term in Eq. (4) gives the decay of the $^1G_4$ luminescence using t_2 and γ parameters and the second term gives the risetime (t_3) of the $^1G_4$ luminescence for the case where $t_3 < t_2$. The decay time of the $^1G_4$ level that contains the slow component of the $Yb^{3+} \rightarrow Pr^{3+}$ ET as well as BT (i.e, $Pr^{3+} \rightarrow Yb^{3+}$) was obtained by

$$\tau_2 = \frac{1}{B}\int I_2(t)\mathrm{d}t + t_3. \tag{5}$$

The following parameters were obtained from a best fit: (i) $x = 1$ mol. %: $t_3 = 2.54$ μs, $t_2 = 607$ μs and $\gamma = 97$ s^{-1} ($R^2 = 0.996$) and $\tau_2 = 136$ μs; (ii) $x = 2$ mol. %: $t_3 = 2.64$ μs, $t_2 = 217$ μs and $\gamma = 49$ s^{-1} ($R^2 = 0.997$) and $\tau_2 = 124$ μs; (iii) $x = 3$ mol. %: $t_3 = 2.85$ μs, $t_2 = 127$ μs and $\gamma = 77$ s^{-1} ($R^2 = 0.999$) and $\tau_2 = 105$ μs; (iv) $x = 4$ mol. %: $t_3 = 3.13$ μs, $t_2 = 94.6$ μs and $\gamma = 0$ ($R^2 = 0.999$) and $\tau_2 = 95$ μs; and (v) $x = 5$ mol. %: $t_3 = 3.36$ μs, $t_2 = 76.2$ μs and $\gamma = 0$ ($R^2 = 0.998$) and $\tau_2 = 76.2$ μs.

The ET process that accounts for the slow component to the $Yb^{3+} \rightarrow Pr^{3+}$ ET is due to partial $Yb^{3+} \rightarrow Pr^{3=}$ ET that is assisted by hopping processes among the excited Yb^{3+} ions

whose time constant can be evaluated using the following relation $B\tau_2 = B\tau(\text{slow}) + B\tau_1$ between the total and partial luminescence decay areas (or integrated values) giving

$$\tau(\text{slow}) = \tau_2 - \tau_1, \tag{6}$$

where τ_2 is the total decay (integrated value) of $^1G_4$ level measured after excitation at 970 nm that includes the slow component of the $Yb^{3+} \rightarrow Pr^{3+}$ ET, BT ($Pr^{3+} \rightarrow Yb^{3+}$), and the intrinsic decay time of the $^1G_4$ level. τ_1 is the integrated lifetime of $^1G_4$ level measured after 442 nm excitation that includes the intrinsic decay time of the $^1G_4$ level and BT ($Pr^{3+} \rightarrow Yb^{3+}$). The slow transfer rates (in s^{-1}) of $Yb^{3+}(x) \rightarrow Pr^{3+}(1)$ were calculated using the relation $W_T(\text{slow}) = \frac{1}{\tau(\text{slow})} - \frac{1}{\tau_i(^2F_{5/2})}$ whose values are given in Table 1. The measured transfer rate of 2.64×10^4 s^{-1} (for the slow component) for $Yb^{3+}(5):Pr^{3+}(1)$-codoped ZBLAN is close to the value of 1.75×10^4 s^{-1} as reported previously in the literature [7] for $Yb^{3+}(5)$, $Pr^{3+}(0.75)$:YAP; however, the fast component of the $Yb^{3+} \rightarrow Pr^{3+}$ ET was not observed in this previous study, which may be a result of the avalanche type excitation, i.e., $Yb^{3+} \rightarrow Pr^{3+}$ ($^3P_0$), produced by the nonresonant laser excitation at 854 nm. Figure 6(b) shows the $Yb^{3+} \rightarrow Pr^{3+}$ rate W_T (slow) (in s^{-1}) obtained using Eq. (6) for $x = 1$, 2, 3, 4, and 5 mol. %. The quadratic dependence of W_T (slow) on x is expected for ET processes involving a random walk that is assisted by excitation migration given that both ET rates are dependent [10].

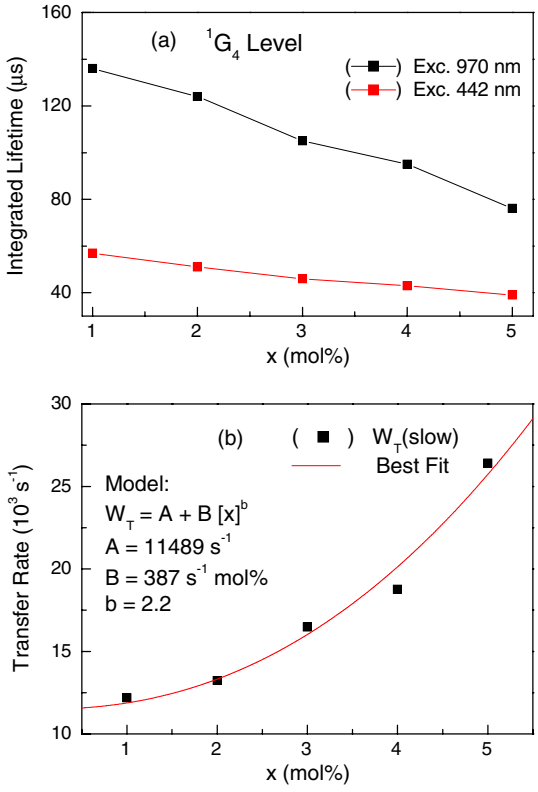

Fig. 6. (a) Shows the integrated lifetime of the $^1G_4$ level (τ_1) obtained from Eq. (2) for the $Yb^{3+}(x):Pr^{3+}$(1 mol. %) systems. (b) Transfer rate W_T (slow) (s^{-1}) obtained using Eq. (5).

The luminescence risetime t_3 is consistent with the fast component to the $Yb^{3+} \rightarrow Pr^{3+}$ ET process because t_3 is larger than the response time of the InSb detector (~0.5 μs), as can be seen in Fig. 7. One can therefore take the ET rate using

$$W_T(\text{fast}) = \frac{1}{t_3} - \frac{1}{\tau_i(^2F_{5/2})}, \tag{7}$$

where τ_i ($^2F_{5/2}$) is equal to 2.13 ms (i.e., the intrinsic lifetime). We have seen that the risetime (t_3) of the $^1G_4$ level is due to $Yb^{3+} \rightarrow Pr^{3+}$ ET (assisted by fast migration) and observed a linear increase in t_3 with increasing [Yb^{3+}], as shown in Fig. 8(a). This behavior may indicate that excitation migration involves some trapping effects that would increase t_3 as x increases. Figure 8(b) shows the W_T (fast) rate's dependence on [Yb^{3+}]. An estimative of the fraction of the $Yb^{3+} \rightarrow Pr^{3+}$ ET that relates to the slow component was carried out using the relation derived from the luminescence decay areas $f = \frac{\tau(\text{slow})}{\tau_1(^1G_4) + \tau(\text{slow})}$, where f values were 0.58 for $x = 1$, 0.58 for $x = 2$, 0.56 for $x = 3$, 0.54 for $x = 4$, and 0.5 for $x = 5$ with an average value $f = 0.55$.

The nonradiative multiphonon relaxation rate from the $^1G_4$ level to the $^3F_4$ level is obtained using the relation $W_{nR} = \frac{1}{\tau_i(^1G_4)} - \frac{1}{\tau_R}$ with $\tau_R = 2.43$ ms [11] and τ_i ($^1G_4$) = 67 μs (the intrinsic lifetime of $^1G_4$ level measured in this work) providing $W_{nR} = 14514$ s^{-1}. Our intrinsic value measured for the $^1G_4$ level (67 μs) is shorter than one previously reported in [12] of 107 μs for Pr^{3+}-doped ZBLAN glass; however, no experimental luminescence decay curve was shown for this level nor the experimental conditions under which the lifetime measurements were made.

C. Upconversion Luminescence from the $^3P_0$ Level

The upconversion luminescence spectrum has been measured for a sample with $x = 5$ mol. % after laser excitation at 970 nm with a pulse average energy of 11.8 mJ, pulse repetition rate of 10 Hz and 4 ns pulse width. Figure 9 shows five main peaks in the luminescence located at 481, 521, 603, 636, and 717 nm, which were attributed to emission from the $^3P_0$ level to the

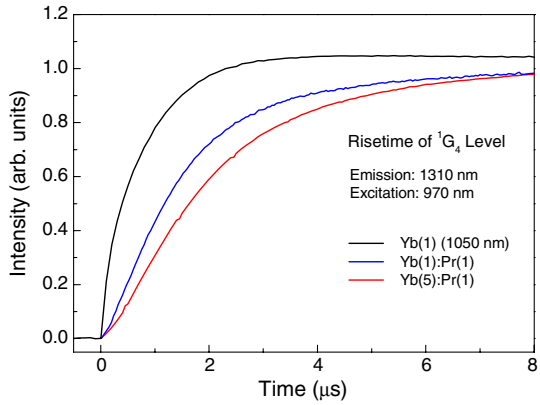

Fig. 7. Measured risetime (t_3) of the 1310 nm luminescence from the $^1G_4$ excited level after the laser excitation at 970 nm for Yb^{3+}(1 mol. %):Pr^{3+}(1 mol. %) and Yb^{3+}(5 mol. %):Pr^{3+}(1 mol. %) systems. A comparison is made with the $^2F_{5/2}$ level emission at 1000 nm measured for Yb^{3+}(1 mol. %)-doped ZBLAN for comparison.

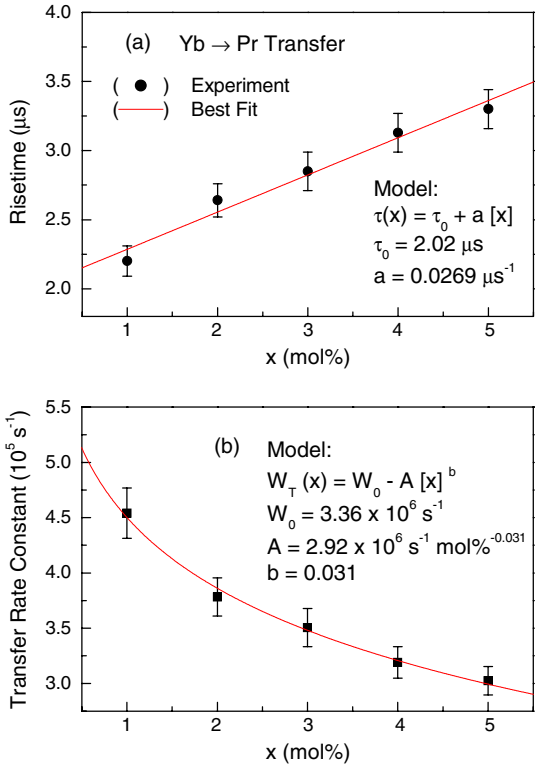

Fig. 8. (a) Shows the measured risetime constant (t_3) of the $^1G_4$ after laser excitation at 970 nm. A linear increase in t_3 with increasing [Yb^{3+}] is observed that is consistent with excitation migration trapping effects expected for higher Yb^{3+} concentrations. (b) Shows the $Yb^{3+} \rightarrow Pr^{3+}$ transfer probability, W_T (fast) (s^{-1}) as a function of [Yb^{3+}] (or x mol. %).

$^3H_4$, $^3H_4$, $^3H_3$, $^3F_2$ and $^3F_3$ levels, respectively. The upconversion process was induced by the $^2F_{5/2}(Yb^{3+}) \times {}^1G_4(Pr^{3+})$ crossover dipole–dipole interaction with ET from to $^3P_0$ level relaxing to the $^2F_{7/2}(Yb^{3+}) + {}^3P_0(Pr^{3+})$ configuration to produce anti-Stokes emission, which is shown in Fig. 9.

The characteristics of the upconversion process were investigated using the 603 nm luminescence (from the $^3P_0$ level) as a probe after laser excitation at 970 nm (with $E = 11.8$ mJ and the $x = 5$ mol. % sample). The measured emission transient is presented in Fig. 10 (see the black line), where it is

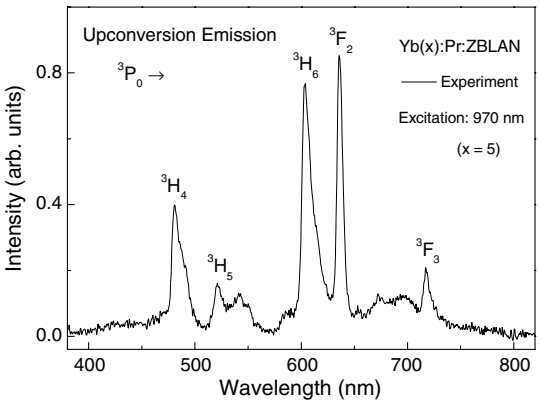

Fig. 9. Measured upconversion luminescence spectrum measured for Yb^{3+}(5 mol. %), Pr^{3+}(1 mol. %)-doped ZBLAN induced by laser excitation at 970 nm (10 Hz, 4 ns), and detected using a HR 2000 spectrometer with a CCD connected to an fiber optical.

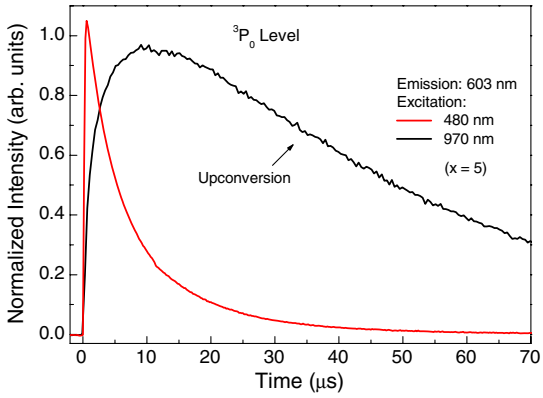

Fig. 10. Measured upconversion luminescence transient of the $^3P_0$ level measured at 603 nm in Yb^{3+}(5 mol. %), Pr^{3+}(1 mol. %)-doped ZBLAN after laser excitation at 970 nm (red solid line) and after laser excitation at 480 nm (black solid line). The risetime of the upconverted 603 nm emission is similar to the decay time of the $^3P_0$ level that is $\tau = 6.8$ μs for $x = 5$ mol. %.

observed that the upconversion luminescence at 603 nm has a risetime (t_3) similar to the decay time of the 603 nm fluorescence ($\tau = 6.8$ μs) determined after direct excitation at 480 nm (see the red line in this figure). From this observation, we conclude that the upconversion process is responsible for the long decay component of the 603 nm luminescence after laser excitation at 970 nm, which is shown in Fig. 11 for the $x = 1$, 2, 3, 4, and 5 mol. % samples. The upconverted 603 nm luminescence presented in Fig. 11 was fitted using an empirical relation similar to Eq. (4) that has been used to fit upconversion luminescence transients with success in Er^{3+} and Yb^{3+}, Tm^{3+}-codoped fluoride crystals [13–15]. The effective time constant of the upconversion luminescence was obtained by the integration in Eq. (5). The results are (i) $\tau_{up} = 99$ μs (for $x = 1$ mol. %); (ii) $\tau_{up} = 91$ μs (for $x = 2$ mol. %); (iii) $\tau_{up} = 70$ μs (for $x = 3$ mol. %); (iv) $\tau_{up} = 57$ μs (for $x = 4$ mol. %); and (v) $\tau_{up} = 46$ μs (for $x = 5$ mol. %).

The upconversion transfer rate (W_{UP}) was obtained using

$$W_{UP} = \frac{1}{\tau_{uP}} - \frac{1}{\tau_2} - \frac{1}{\tau_i(^2F_{5/2})}, \tag{8}$$

where τ_2 is the total integrated lifetime of the $^1G_4$ level in $Yb^{3+}(x)$:$Pr^{3+}(1)$ samples measured after laser excitation at

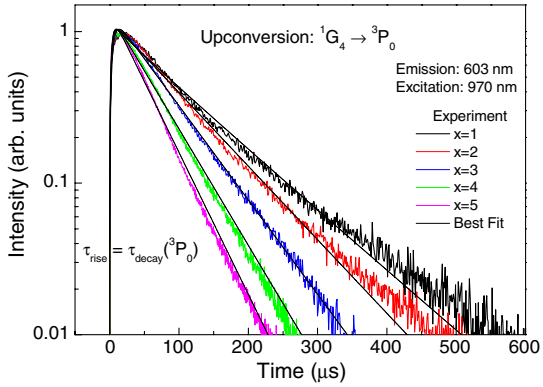

Fig. 11. Measured upconversion luminescence transient of the $^3P_0$ level measured at 603 nm for $Yb^{3+}(x)$, Pr^{3+}(1 mol. %)-doped ZBLAN after laser excitation at 970 nm (T = 300 K) with an average pulse energy of 11.8 mJ.

970 nm, which is equal to 136 μs (for $x = 1$ mol. %), 124 μs (for $x = 2$ mol. %), 105 μs (for $x = 3$ mol. %), 95 μs (for $x = 4$ mol. %), and 76 μs (for $x = 5$ mol) and τ_i ($^2F_{5/2}$) = 2.13 ms. Because the upconversion process is created by the $^2F_{5/2}(Yb^{3+}) \times {}^1G_4(Pr^{3+})$ crossover interaction, an intermediate donor state is produced having a equivalent decay rate equal to $W_{donor}(s^{-1}) = [1/\tau_2 + 1/\tau_i(^2F_{5/2})]$, which justifies the subtracted terms applied in Eq. (8).

Because the upconversion process involves two interacting excited states and ET, the probability rate of upconversion may depend on the excitation intensity whose experimental results are shown in Fig. 12(a) for $x = 1$ and 12(b) for $x = 5$ (solid squares). One can observe that W_{UP} increases with increasing excitation density N^* (i.e., Yb^{3+} excited ions per cm^3) and tends to a constant rate K_0 for $N^* \geq 3 \times 10^{18}$ excited ions cm^{-3}. This behavior has been observed for ET upconversion processes in Ho^{3+}-doped ZBLAN and Er^{3+}-doped tellurite glass with the critical radius model being used to explain this mechanism. [16,17] The critical radius model was used to fit the W_{UP} behavior as a function of the excitation density (N^*), which provided the parameters: (i) $K_0 = 1748\ s^{-1}$ and $N_C = 1.2 \times 10^{18}\ cm^{-3}$ (for $x = 1$ mol. %) and (ii) $K_0 = 9250\ s^{-1}$ and $N_C = 3.4 \times 10^{17}\ cm^{-3}$ (for $x = 5$ mol. %). Figure 13 shows the K_0 upconversion rate constant as a function of [Yb^{3+}] where a linear behavior is observed.

D. Cross-Relaxation from the $^3P_0$ Level

The luminescence decay of the $^3P_0$ level was investigated in $Yb^{3+}(x)$:Pr^{3+}(1 mol. %) and Pr^{3+}(1 mol. %) systems using resonant $^3H_6 \rightarrow {}^3P_0$ laser excitation at 480 nm. It was observed

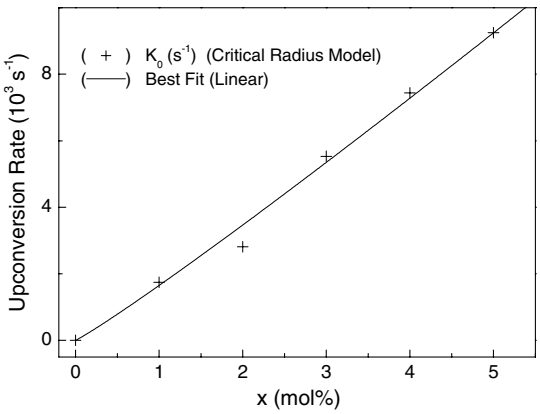

Fig. 13. Rate constant values K_0 (in s^{-1}) obtained from a best fit using the critical radius model for the upconversion process shown in Fig. 12 as a function [Yb^{3+}] where a linear dependence of K_0 with increasing of x is observed.

that the Pr^{3+}(1 mol. %) system displayed exponential decay with a lifetime of 35 μs, while for the $Yb^{3+}(x)$:Pr^{3+}(1 mol. %) system, the luminescence decays were fitted using Eq. (1), which provided the following parameters: (i) $t_1 = 28.6$ μs and $\gamma = 29.6\ s^{-1/2}$ giving $\tau = 25$ μs (for $x = 1$ mol. %); (ii) $t_1 = 24.4$ μs and $\gamma = 96.6\ s^{-1/2}$ giving $\tau_1 = 16.4$ μs (for $x = 2$ mol. %); (iii) $t_1 = 31.9$ μs and $\gamma = 256.2\ s^{-1/2}$ giving $\tau = 10.7$ μs (for $x = 3$ mol. %); (iv) $t_1 = 15$ μs and $\gamma = 261\ s^{-1/2}$ giving $\tau = 8.3$ μs (for $x = 4$ mol. %); (v) $t_1 = 18$ μs and $\gamma = 226\ s^{-1/2}$ giving $\tau = 6.76$ μs (for $x = 5$ mol. %), where τ was

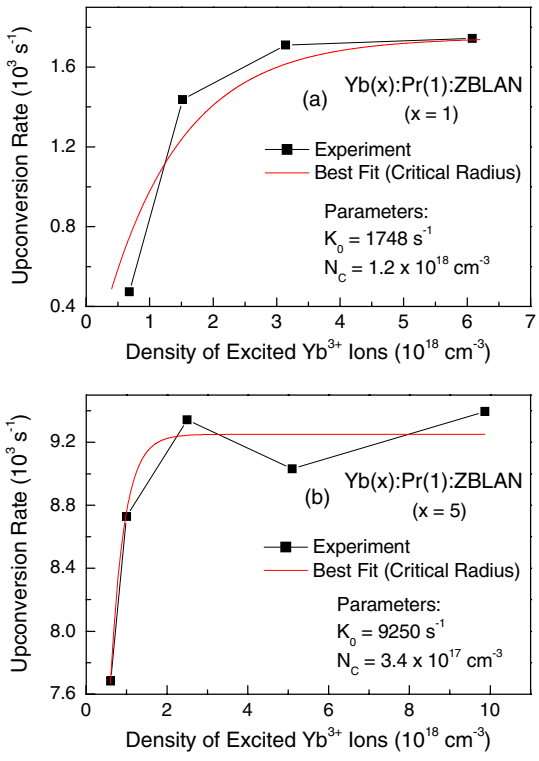

Fig. 12. Upconversion rate, W_{UP} (s^{-1}), as a function of the density of excited Yb^{3+} ions for (a) $x = 1$ mol. % and (b) $x = 5$ (b) samples. A best fit was done using the critical radius model [16] that is represented by the red lines.

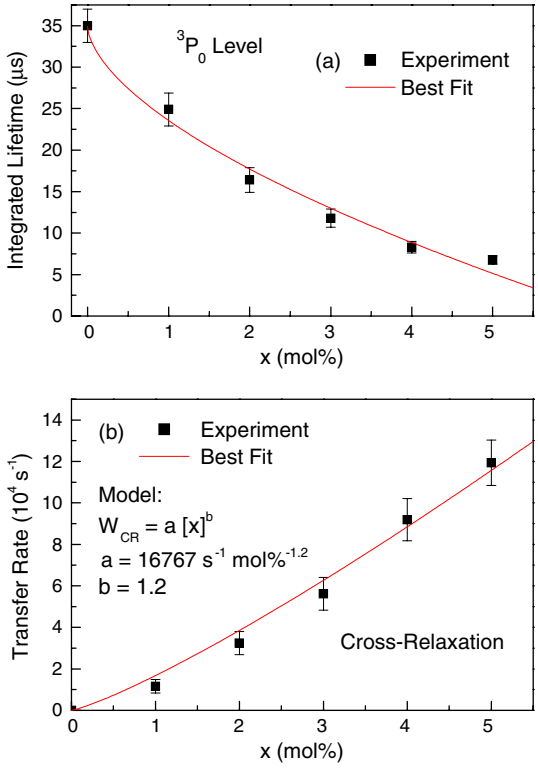

Fig. 14. (a) Measured integrated lifetime of the $^3P_0$ level (τ_1) obtained from Eq. (2) for the $Yb^{3+}(x)$:Pr^{3+}(1 mol. %)) system after laser excitation at 480 nm. $\tau_1 = 35$ μs was determined for Pr^{3+}(1 mol. %)-doped ZBLAN as the intrinsic lifetime of the $^3P_0$ level. (b) The CR rate W_{CR} (s^{-1}) obtained using Eq. (9).

obtained by integration of Eq. (2). Figure 14(a) shows the decreasing decay time (τ) of the $^3P_0$ level with increasing [Yb^{3+}]. This effect indicates that the nonradiative decay of the $^3P_0$ level of Pr^{3+} is introduced by a crossover interaction between Pr^{3+} and the Yb^{3+} ions. This relaxation process must be due to the $^3P_0(Pr^{3+}) \times {}^2F_{7/2}(Yb^{3+})$ interionic dipole–dipole interaction, which relaxes the system to the $^1G_4(Pr^{3+}) + {}^2F_{5/2}(Yb^{3+})$ electronic configuration. The CR rate (in s^{-1}) can be obtained using Eq. (9),

$$W_{CR} = \frac{1}{\tau} - \frac{1}{\tau_i(^3P_0)}, \tag{9}$$

where τ_i ($^3P_0$) = 35 μs is the intrinsic lifetime that provided the values for W_{CR} (in s^{-1}) shown in Fig. 14(b). The intrinsic lifetime for the $^3P_0$ level of 35 μs is consistent with the value of 45 μs found in the literature for Pr^{3+}-doped fluoroindate glass. [18] One can observe that W_{CR} exhibits a quasi-linear dependence on [Yb^{3+}] with a potential factor b equal to 1.2.

4. DISCUSSION

In order to test the viability of Yb^{3+}, Pr^{3+}-doped ZBLAN glass as a gain medium for fiber lasers, we will use a rate equation analysis to describe the CW pumping of $Yb^{3+}(x)$:Pr^{3+}(1 mol. %)-doped ZBLAN. Figure 15 shows the simplified energy level scheme used to describe the Yb^{3+}, Pr^{3+}-doped ZBLAN fiber laser system for CW pumping of the $^2F_{5/2}$ level (n_2). n_1 and n_2 are the populations of the $^2F_{7/2}$, $^2F_{5/2}$ energy levels of Yb^{3+}, n_3, n_4 and n_5 are the populations of the $^3H_4$, $^1G_4$, and $^3P_0$ energy levels of Pr^{3+}, respectively, and $n_1 + n_2 = 1$ and $n_3 + n_4 + n_5 = 1$.

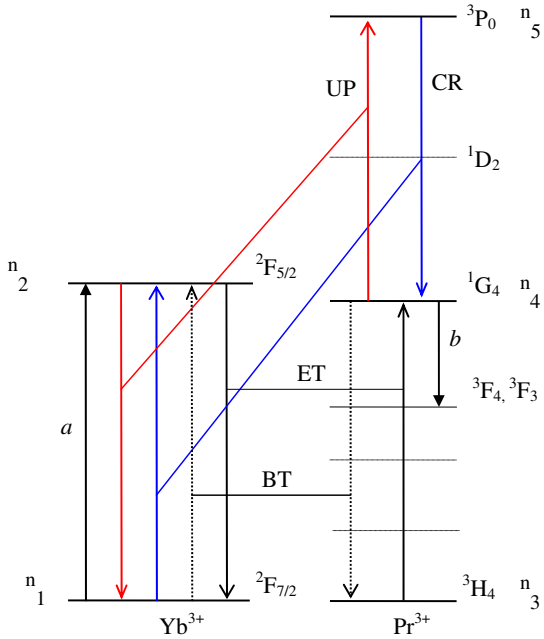

Fig. 15. Energy level diagram for Yb^{3+}, Pr^{3+}-codoped ZBLAN used for the rate equation modeling of optical pumping of the $^2F_{5/2}$ level at 970 nm. *a* represents the 3600 nm laser emission, *b* represents the $^1G_4$, ET represents direct energy transfer, BT represents back transfer, upconversion represents upconversion, and CR represents cross-relaxation. Note that the populations of the $^3F_4$, $^3F_3$ levels of Pr^{3+} are negligible due to strong multiphonon relaxation to the next $^3H_6$ level.

The populations of the $^3H_5$, $^3H_6$, and $^3F_2$ levels were considered negligible in ZBLAN because of strong nonradiative decay of these levels by multiphonon relaxation. The rate equations for the simplified system for 970 nm pumping are

$$\frac{dn_1}{dt} = -R_P n_1 + \frac{n_2}{\tau_{R_2}} + W_T n_2 n_3 - W_{BT} n_1 n_4 + W_{UP} n_2 n_4 - W_{CR} n_1 n_5, \tag{10}$$

$$\frac{dn_2}{dt} = R_P n_1 - \frac{n_2}{\tau_{R_2}} - W_T n_2 n_3 + W_{BT} n_1 n_4 - W_{UP} n_2 n_4 + W_{CR} n_1 n_5, \tag{11}$$

$$\frac{dn_3}{dt} = -W_T n_2 n_3 + W_{BT} n_1 n_4 + \frac{n_4}{\tau_{n4}} + (1 - \beta_{54}) \frac{n_5}{\tau_{n5}}, \tag{12}$$

$$\frac{dn_4}{dt} = W_T n_2 n_3 - W_{BT} n_1 n_4 - W_{UP} n_2 n_4 + W_{CR} n_1 n_5 - \frac{n_4}{\tau_{n4}} + \beta_{54} \frac{n_5}{\tau_{n5}}, \tag{13}$$

$$\frac{dn_5}{dt} = W_{UP} n_2 n_4 - W_{CR} n_1 n_5 - \frac{n_5}{\tau_{n5}}, \tag{14}$$

where $R_P = \sigma_{12} \frac{I_P}{h\nu_P}$ is the pump rate (s^{-1}), I_P is the intensity of the pump light ($W\,cm^{-2}$), and $h\nu_P$ is the photon energy of the pump radiation. σ_{12} is the absorption cross section of Yb^{3+} at 970 nm whose value is $\sigma_{12} = 5.98\ cm \times 10^{-21}$ cm (note we are exploring an excitation wavelength shifted from the maximum absorption at 975 nm, which would allow more penetration depth into the sample). Experimental values of the intrinsic total decay times $\tau_{n2} = \tau_i$ ($^2F_{5/2}$), $\tau_{n4} = \tau_i$ ($^1G_4$), $\tau_{n5} = \tau_i$ ($^3P_0$) and the luminescence branching ratios (β_{31}, β_{32}), the multiphonon decay rates [W_{nR} (43)], and the transfer rates (W_T, W_{BT}, W_{CR} and W_{UP}) as a function of [Yb^{3+}] in ZBLAN are listed in Table 1. The τ_{n2}, τ_{n4}, and τ_{n5} lifetimes were measured in this work.

The calculated $^1G_4$ excited state population n_4 (in mol. %) obtained by numerical simulation of the rate equations for a pumping intensity of 85.5 $kW\,cm^{-2}$ is shown in Fig. 16(a), where one can observe that equilibrium occurs for a time shorter than 1.5 ms. Because forward $Yb^{3+} \rightarrow Pr^{3+}$ ET is divided into two independent transfer processes, i.e., fast (with a 45% contribution) and slow (with a 55% contribution), the numerical simulation should be done considering these two cases and the population n_4 must be calculated using the relation $n_4 = 0.45 \times n_4(\text{fast}) + 0.55 \times n_4(\text{slow})$, where n_4(slow) and n_4(fast) are the partial populations of the $^1G_4$ level obtained by distinct numerical simulations: first making $W_T = W_T$ (slow) and second making $W_T = W_T$ (fast) in the rate equations system and the rate values W_T (fast) and W_T (slow) given in Table 1. The population inversion is given by $\Delta n = n_4$.

At equilibrium, the populations n_3, n_4, and n_5 were taken and the population inversion $\Delta n = n_4$ was obtained for Yb^{3+}, Pr^{3+}-doped ZBLAN as a function of the pump intensity at 970 nm; these results are presented in Fig. 17, which indicates a negligibly small threshold pump intensity for all samples. Figure 17 shows that the population inversion increases almost linearly, where one can see only a small decrease in the

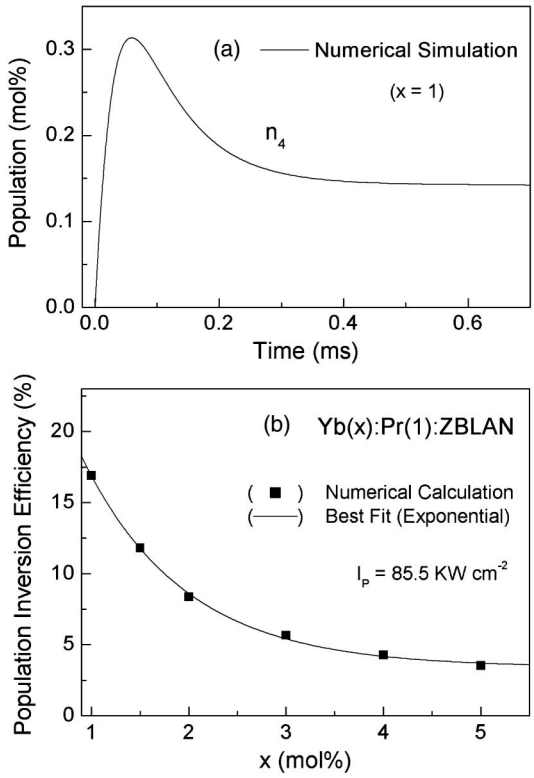

Fig. 16. Calculations of (a) the time evolution of n_4 population (in mol. %) representing the $^1G_4$ showing steady state equilibrium is reached in a time shorter than 0.7 ms. (b) Inversion population efficiency values (%) obtained for $Yb^{3+}(x)$, Pr^{3+}(1 mol.)-doped ZBLAN showing that $x = 1$ mol. % is the most efficient Yb^{3+} concentration.

values of Δn for higher pump intensities (i.e., >80 kW cm^{-2}). We can define, however, the population inversion efficiency according to the relation $E_f = 100 \times \frac{\Delta n(x)}{[n_2(x)]_{y=0}}$, where $[n_2(x)]_{y=0}$ is the population of the $^2F_{5/2}$ excited state of Yb^{3+} obtained at equilibrium for 970 nm CW pumping for the $Yb^{3+}(x)$-doped system where $[Pr^{3+}] = 0$ (or $y = 0$). The results are presented in Fig. 16(b) for a fixed value of pump intensity of 85.5 kW cm^{-2} providing a population inversion efficiency (E_f) of 17% for Yb^{3+} (1 mol. %), Pr^{3+} (1 mol. %)-doped ZBLAN, which should be the best configuration for

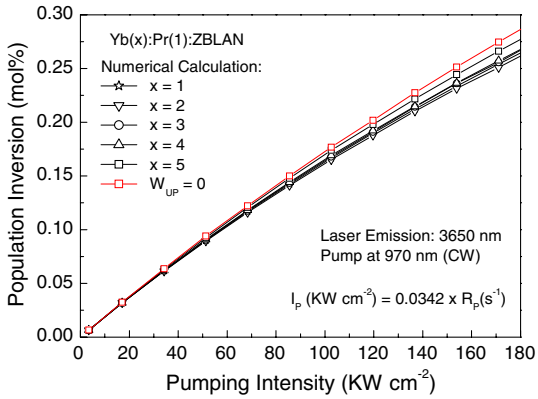

Fig. 17. Calculated population inversion (in mol. %) calculated using numerical solution of rate equations system for $Yb^{3+}(x)$:Pr^{3+} (1 mol. %) samples for CW pumping at 970 nm for several pump intensities (given in kW cm^{-2}). A small effect due to upconversion process is observed for higher pumping intensities.

fiber laser emission at 3.6 μm within the Yb^{3+} concentration range from 1 to 5 mol. %. This effect can be explained based on the fact that the upconversion populates the $^3P_0$ level, which is de-excited by strong cross relaxation, i.e., $Pr^{3+}(^3P_0)\times Yb^{3+}(^2F_{7/2})$, which transfer the $^3P_0$ excitation back to the $^1G_4$ level.

5. CONCLUSIONS

It has been determined that the luminescence efficiency of the $^1G_4 \rightarrow {}^3F_4$, $^3F_3$ transition at ~3.6 μm in $Yb^3(x)$, $Pr^{3+}(1)$-doped ZBLAN glass at $T = 300$ K is 2.8%, which is primarily the result of large rates of multiphonon emission that force the nonradiative decay rate to be 14514 s^{-1} compared to the calculated radiative decay rate of 412 s^{-1}. We have observed that the decay time of the $^1G_4$ level is dependent on $[Yb^{3+}]$, which we attribute to migration-assisted energy BT to the Yb^{3+} ions; however, this transfer rate is small, e.g., 2526 s^{-1} for $x = 1$ mol. %, compared to the rates of direct ET that are of the order of 3.9×10^5 s^{-1} for the fast component; forward ET is most likely assisted by fast energy migration in a similar way to Yb^{3+}, Er^{3+}-doped ZBLAN [9]. However, we have determined that forward $Yb^{3+} \rightarrow Pr^{3+}$ ET has two components: a fast component that accounts for 45% of the total transfer and a slow component that accounts for 55%. Forward ET should be assisted by hopping migration. We observed upconversion processes between Yb^{3+} and Pr^{3+} ions whose rate W_{UP} (in s^{-1}) is dependent on $[Yb^{3+}]$. It was established that upconversion to the $^3P_0$ excited state of Pr^{3+} may have a small detrimental impact on the performance of a Yb^{3+}, Pr^{3+}-doped ZBLAN fiber laser when CW pumped at 970 nm. We have found that the Yb^{3+}(1 mol.%), Pr^{3+}(1 mol.%)) is the most efficient sample for laser emission at ~3.6 μm within the Yb^{3+} concentration range 1 to 5 mol. %. This dopant combination can be applied to the three main emissions that start from the $^1G_4$ level (Pr^{3+}) and that terminate on the $^3H_5$, $^3H_6$, and $^3F_4$, energy levels and emit at 1350, 1985, and 3680 nm, respectively. All these emissions have laser potential with an inversion population given by $\Delta n = n_4$ according to the processes shown in Fig. 15 and have emission cross sections of 4.1×10^{-21} cm^2 for the 1350 nm emission, 4.23×10^{-21} cm^2 for the 1985 nm emission, and 5.76×10^{-21} cm^{-2} for the 3680 nm emission.

ACKNOWLEDGMENTS

S. Jackson acknowledges support from a Queen Elizabeth II Fellowship. The authors are thankful for financial support from FAPESP (Grants N01995/4166-0 and 2000/10986-0), CNPq, and the Australian Research Council.

REFERENCES

1. D. Faucher, M. Bernier, G. Androz, N. Caron, and R. Vallee, "20 W passively cooled single-mode all-fiber laser at 2.8 μm," Opt. Lett. **36**, 1104 (2011).
2. S. D. Jackson, "High-power and highly efficient diode-cladding-pumped holmium-doped fluoride fiber laser operating at 2.94 μm," Opt. Lett. **34**, 2327 (2009).
3. J. Schneider, C. Carbonnier, and U.B. Unrau, "Characterization of a Ho^{3+}-doped fluoride fiber laser with a 3.9 μm emission wavelength," Appl. Opt. **36**, 8595 (1997).
4. A.A. Kaminskii, K. Kurbanov, and T. V. Uvarova, "Stimulated radiation from single-crystals of $BaYb_2F_8Pr^{(3+)}$," Izv. Akad. Nauk SSSR, Sev. Neorgan. Matter **23**, 1049 (1987).

5. A. A. Kaminskii, K. Kurbanov, and A. V. Pelevin, "New channels for stimulated-emission of $Pr^{(3+)}$ ions in tetragonal fluorides LiRF4 with the structure of scheelite," Izv. Akad. Nauk. SSSR, Sev. Neorgan. Matter **23**, 1934 (1987).
6. A. A. Kaminskii, "Progress in praseodymium crystalline lasers emitting in the visible," in *Advanced Solid State Lasers*, A. A. Pinto and T. Y. Fan, eds., Vol. **15**, OSA Proceedings Series (Optical Society of America, 1993), pp. 266–270.
7. S. Kück, K. Sebald, A. Diening, E. Heumann, E. Mix, and G. Huber, "Energy transfer processes in Pr, Yb-doped crystals," in *OSA Trends in Optics and Photonics*, Martin M. Fejer, Hagop Injeyan, and Ursula Keller, eds., Vol. **26**, Advanced Solid State Lasers (Optical Society of America, 1999), pp. 658–663.
8. A. I. Burshtein, "Jump mechanism of energy transfer," Soviet Phys. JETP **35**, 882 (1972).
9. L. D. da Vila, L. Gomes, L. V. G. Tarelho, S. J. L. Ribeiro, and Y. Messaddeq, "Dynamics of Tm–Ho energy transfer and deactivation of the $^3F_4$ low level of thulium in fluorozirconate glasses," J. Appl. Phys. **95**, 5451 (2004).
10. R. C. Powell, "Nonradiative energy-transfer: multistep process," in *Physics of Solid-State Laser Materials* (Springer, 1998), pp. 193–203.
11. W. Seeber, E. A. Downing, L. Hesselink, M. M. Fejer, and D. Ehrt, "Pr^{3+}-doped fluoride glasses," J. Non-Crystalline Solids **189**, 218 (1995).
12. W. G. Jordan, Animesh Jha, M. Lunt, S. T. Davey, R. Wyatt, and W. J. Rothwell, "The optical properties of ZrF4-based glasses with extended Pr^{3+}:$^1G_4 \rightarrow {}^3H_5$ fluorescence lifetimes," J. Non-Crystalline Solids **184**, 5 (1995).
13. L. Gomes, A. F. H. Librantz, F. H. Jagosich, L. A. W. Alves, I. M. Ranieri, and S. L. Baldochi, "Energy transfer rates and population inversion of $^4I_{11/2}$ excited state of Er^{3+} investigated by means of numerical solutions of the rate equations system in Er:LiYF4 crystal," J. Appl. Phys. **106**, 103508 (2009).
14. A. F. H. Librantz, L. Gomes, L. C. Courrol, I. M. Ranieri, and S. L. Baldochi, "Population inversion of $^1G_4$ excited state of Tm^{3+} investigated by means of numerical solutions of the rate equations system in Yb:Tm:Nd:$LiYF_4$ crystal," J. Appl. Phys. **105**, 113503 (2009).
15. H. Marconi da Silva, M. D. Linhares, A. F. H. Librantz, L. Gomes, L. C. Courrol, S. L. Baldochi, and I. M. Ranieri, "Energy transfer rates and population inversion investigation of $^1G_4$ and $^1D_2$ excited states of Tm^{3+} in Yb:Tm:Nd:KY_3F_{10} crystals," J. Appl. Phys. **109**, 083533 (2011).
16. A. F. H. Librantz, S. D. Jackson, F. H. Jagosich, L. Gomes, G. Poirier, S. J. L. Ribeiro, and Y. Messaddeq, "Excited state dynamics of the Ho^{3+} ions in holmium singly doped and holmium, praseodymium-codoped fluoride glasses," J. Appl. Phys. **101**, 123111 (2007).
17. L. Gomes, M. Oermann, H. E. Heidepriem, D. Ottaway, T. Monro, A. F. H. Librantz, and S. D. Jackson, "Energy level decay and excited state absorption processes in erbium-doped tellurite glass," J. Appl. Phys. **110**, 083111 (2011).
18. A. B. Arauzo, R. Cases, and R. Alcalá, "Optical absorption, photoluminescence and cross relaxation of Pr^{3+} ion in some fluoride glasses," Phys. Chem. Glasses **35**, 202 (1994).